Acta Cryst. (1979). B35, 1776–1785

The Structure of α-Chymotrypsin. II. Fourier Phase Refinement and Extension of the Dimeric Structure at 1·8 Å Resolution by Density Modification

BY N. V. RAGHAVAN AND A. TULINSKY

Department of Chemistry, Michigan State University, East Lansing, Michigan 48824, *USA*

(*Received* 1 *November* 1978; *accepted* 8 *February* 1979)

Abstract

The phase angles of the α-chymotrypsin (α-CHT) dimer have been extended from 2·8 Å to 1·8 Å resolution by Fourier phase refinement and electron density modification *via* fast Fourier transform methods. The data set was collected from two crystals, both of which showed less than 10% intensity decay with X-ray exposure. Of the approximately 39 200 reflections at 1·8 Å resolution, about 19 700 have observable intensities which were measured with a Picker FACS-I diffractometer employing a 'wandering' ω-step-scan procedure. Refinement extension by density modification began with the 2·8 Å resolution multiple isomorphous replacement (MIR) phases (8 500 with $m > 0{\cdot}3$) using a modification function suggested by Collins (1975). Convergence was attained in seven cycles of refinement extension and the original MIR phase set was expanded to 19 066 reflections (97% of the observed data). The average change in phase angle for the last cycle was 3·8° while the average change in phase angle from the 2·8 Å resolution MIR set was 28°. The latter compares well with the average error expected in MIR phases ($\langle m \rangle = 0{\cdot}76$, ~40°). The position of the local twofold axis has been refined at 1·8 Å resolution by the method of least squares minimizing the sum of the squares of the difference density between the independent molecules of the asymmetric unit. The correlation coefficient decreased at increased resolution indicating an increased lack of twofold symmetry. The 2·8 Å and 1·8 Å resolution maps have been compared and the general increase in quality is discussed.

1. Introduction

The structure of α-chymotrypsin (α-CHT) determined from crystals grown between pH 3·0–4·0 (pH 3·6 conformer; Mavridis, Tulinsky & Liebman, 1974) possesses two molecules per asymmetric unit and these correspond to the associated dimeric form of the enzyme which is observed in solution at lower pH values (Aune & Timasheff, 1971). We have determined the dimeric structure at 2·8 Å resolution by the multiple isomorphous replacement method (MIR) using six heavy-atom derivatives and with anomalous-scattering measurements from one of these (Tulinsky, Mani, Morimoto & Vandlen, 1973; hereafter referred to as part I). The two molecules of the dimer are related by a local non-crystallographic twofold rotation axis approximately parallel to the **a*** direction of the crystal (Blow, Rossmann & Jeffery, 1964). The structures of the independent molecules have been compared and the significant structural and behavioral differences which exist between them at 2·8 Å resolution have been discussed (Tulinsky, Vandlen, Morimoto, Mani & Wright, 1973; Vandlen & Tulinsky, 1973; Mavridis, Tulinsky & Liebman, 1974; Tulinsky, Mavridis & Mann, 1978).

Although the isomorphous derivatives used to determine the 2·8 Å resolution structure were of comparatively excellent quality, there were clear indications during the least-squares refinement of the heavy-atom parameters of the derivatives that the underlying assumption of isomorphism was beginning to deteriorate in the higher-order data (part I). Thus, we confined our original MIR work to 2·8 Å resolution even though a MIR structure for tosyl-α-CHT at 2·0 Å resolution had been reported earlier (Birktoft & Blow, 1972). The isomorphism among the heavy-atom derivatives of the latter (Blow & Matthews, 1973) does not appear to be any better than that of our 2·8 Å resolution native derivatives so that the 2·0 Å resolution work was justified to the extent that the electron density of the independent molecules of the asymmetric unit was averaged about the local twofold axis and only the averaged structure was essentially discussed.

In an effort to avoid the problems associated with lack of isomorphism in the MIR method and the decrease in phasing power of heavy-atom derivatives at higher resolution, we chose to extend the phase angles of α-CHT from 2·8 Å to 1·8 Å resolution by alternate cycles of electron density modification and Fourier inversion (Collins, Brice, la Cour & Legg, 1976). In this way, the extension of phases was accomplished directly

0567-7408/79/081776-10$01.00

and independently of the knowledge of the structure and thus did not bias the latter in the way of assumptions and possible models. Such a procedure was all the more important since we were interested in establishing the details of small structural differences leading to variability or asymmetry in the tertiary structure of the dimer.

Similar phase-extension procedures have been used previously by others in the linear form (Hoppe, Gassmann & Zechmeister, 1970), using 'positivity' (Kartha, 1969) and 'positivity and squaring' (Barrett & Zwick, 1971). The least-squares refinement of Sayre's (1974) equation was also considered by us as a possible means of obtaining phase angles without assuming a particular molecular structure. However, the computational requirements of the 1·8 Å resolution α-CHT problem proved too formidable for practical application.

2. Experimental

Prior to three-dimensional data collection proper, a preliminary set of intensity data was collected between 2·8 and 1·8 Å resolution (2θ = 32–50°) in order to determine the indices of the observable reflections. This was accomplished with Cu $K\alpha$ radiation (X-ray tube operating at 160 W, 4 mA) using a 'quick' wandering count 6–drop 2 ω-step-scan procedure (count of 2 s/step) (Wyckoff, Doscher, Tsernoglou, Inagami, Johnson, Hardman, Allewell, Kelly & Richards, 1967; part I) with a Picker FACS I diffractometer equipped with a 32 K disc, seven-track magnetic tape, 650 mm crystal–detector He tube and balanced Ni/Co filters.* A total of about 28 400 reflections were measured, of which about 10 800 were liberally considered to be observable. The observable limit was determined from the histogram shown in Fig. 1, where the number of reflections of a given intensity is plotted against intensity for the weaker reflections. The discontinuity

* For more details of the data-collecting procedures, see part I.

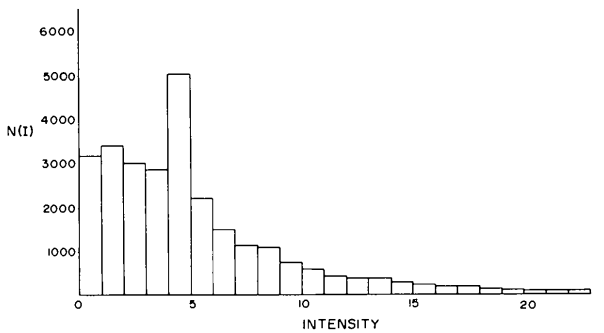

Fig. 1. Distribution of intensities of weaker reflections (I < 23 counts/8 s) between 2·8 and 1·8 Å resolution. $N(I)$ is the number of reflections with intensity I.

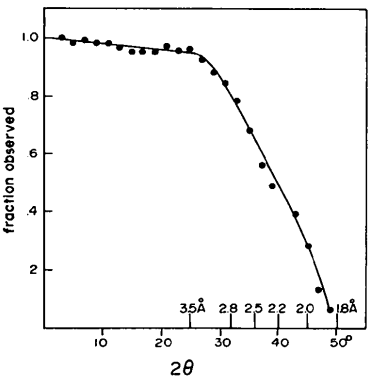

Fig. 2. Fraction of observable intensity data with Bragg angle.

at 5 counts/8 s occurs at background level. The latter was also arrived at independently from a comparison of heights of strip chart recordings.

The three-dimensional intensity data proper were collected using identical conditions and procedures to the foregoing except that (1) a fresh crystal was employed, (2) the counting time was increased to 4 s/step, and (3) only the reflections previously determined as observable were measured (I > 5 counts). The data were collected in three concentric shells of 2θ, with each shell containing approximately 4 000 reflections. The 43–50° shell was collected first, followed by the 40–43° and then the 32–40°. Under our instrumental operating conditions and mode of operation, the intensities of three monitored reflections ($2\theta \sim 32°$) decreased by less than 10% after approximately 123 h of X-ray exposure to the crystal (time taken to measure about 11 150 reflections).

Since the original 2·8 Å resolution set of native intensity data was measured using seven different crystal specimens (part I), in the best interests of the high-resolution work, these data were remeasured. This was accomplished using another fresh crystal, which also proved to show less than 10% intensity decay after about 134 h of exposure. Of the approximately 11 000 reflections measured at 2·8 Å resolution, about 300 overlapped those of the previous crystal and 9871 were taken as observable (92·2%). Of the 39 000 or so reflections at 1·8 Å resolution, 19 757 (~51%) were observed. A curve summarizing the observability of the diffraction pattern of α-CHT is shown in Fig. 2 from which it can be seen that the fraction of observable intensity data falls off rapidly after 2·8 Å resolution. Near the 1·8 Å resolution limit (2θ = 48–50°), only 240 reflections were observed out of about 4000 (5·7%). At higher resolution, reflections become even more radically scarce.

3. Data reduction

The corrections applied to the observed intensities to convert them to structure amplitudes were similar to

those used previously and are described in detail in part I. A summary of the pertinent values and information describing the crystals and corrections is given in Table 1.

The present 2·8 Å resolution intensity-data set, collected from one crystal, was converted to structure amplitudes and scaled to the original seven-crystal data set by comparing the 6·0 Å resolution ($h0l$) electron density projections of the two (part I). The three-dimensional radial $|F|^2$ distributions of the two sets at 2·8 Å resolution were then compared. The scale between the two was within error but the apparent average isotropic thermal parameter of the present data set was about 3·4 Å^2 smaller, giving the data an average overall isotropic B value of 23·6 Å^2 with respect to atoms at rest. After application of a correction for the difference in fall-off between the two data sets, the R value between them was 0·054, where $R = \sum||F_1| - |F_2||/\sum|F_1|$ and the subscripts denote the independent data sets. This value compares favorably with comparisons among the original data (part I). A three-dimensional 'best' difference electron density map was computed using coefficients $m\Delta F \exp(i\alpha_{MIR})$, where m is the figure of merit of a reflection (Blow & Crick, 1959), $\Delta F = (|F_1| - |F_2|)$ and α_{MIR} is the MIR phase angle. The map contained only three small features which attained heights of ±0·08 e Å^{-3}, further indicating that the amplitudes between the two sets of data are very similar and properly placed on the same scale.

The structure amplitudes between 2·8 and 1·8 Å resolution were placed on the same scale as the new 2·8 Å resolution data by comparing a 6·0 Å resolution ($h0l$) electron density projection measured prior to three-dimensional data collection with that of a similar one of the 2·8 Å resolution set. After scaling, the R value for the approximately 300 overlapping reflections near $2\theta = 32°$ was 0·014, confirming the scale so determined and indicating that the average fall-off of the reduced intensity data is the same for both crystals. The three-dimensional 1·8 Å resolution radial $|F|^2$ distribution was plotted and, from the slope of the Wilson line calculated using the empirical formula of α-CHT, an apparent average isotropic thermal parameter was calculated to be in the range 13–16 Å^2 based on the high-order reflections. This value is considerably smaller than those determined using 2·8 Å resolution data alone.

4. Phase refinement

Before the phase angles were extended to 1·8 Å resolution, the 2·8 Å resolution MIR phases were refined by modifying the MIR 'best' electron density. The modification function was based upon that suggested by Collins (1975):

$$\rho_c(\mathbf{r}) = \begin{cases} 3\rho_o^2(\mathbf{r}) - 2\rho_o^3(\mathbf{r}); \text{ for } \rho_o > 0 \\ 0; \text{ for } \rho_o \leq 0, \end{cases} \quad (1)$$

where the observed density, ρ_o, is normalized so as to have a maximum magnitude of 1·0. The refinement procedure consisted of (1) computing a 'best' electron density map using MIR phases with $m > 0{\cdot}3$, (2) modifying the map with function (1) and then calculating $|F_c'|$ and α_c by Fourier inversion, (3) scaling $|F_c'|$ to the same scale as $|F_o|$ giving a scaled $|F_c|$ and computing a new electron density map with $(2|F_o| - |F_c|)$ as amplitudes and α_c as phase angles for all reflections satisfying $|F_c|/|F_o| > C$, where C, the acceptance criterion, is somehow appropriately chosen, and (4) repeating steps (2) and (3) on a $(2|F_o| - |F_c|)$ map until convergence is attained.

The 'best' MIR 2·8 Å resolution map with reflections $m > 0{\cdot}3$ (8400 reflections) was computed with a space-group-specific fast Fourier transform program (Ten Eyck, 1973).* The maximum electron density of this map was 2·48 e Å^{-3} whereas the remainder averaged near 1·5 e Å^{-3}, with a r.m.s. error of 0·18 e Å^{-3} (Dickerson, Kendrew & Strandberg, 1961). If modification function (1) is used repeatedly in the phase refinement of such a map, it will cause a spurious growth of the highest-density regions at the expense of the remainder of the density (Collins, Brice, la Cour & Legg, 1976). Thus, function (1) must be changed in a manner so as to avoid such behavior. One way to accomplish this is as follows: let χ be the value of the normalized density which is related to that density which is barely significant. Function (1) is then scaled

* The space-group specificity leads to a gain of about a factor of 2 in computing time per cycle. For instance, the phase extension to 18 400 reflections at 1·5 Å resolution of staphylococcal nuclease required about 20 min per cycle (Collins, Cotton, Hazen, Meyer & Morimoto, 1975), whereas a similar calculation in the present work required only 11 min per cycle on a comparable computer (CDC 6500).

Table 1. *Summary of pertinent quantities describing the data-collection crystals*

Crystal	Resolution range (Å)	Size (mm)	Absorption*	Crystal: twin ratio	Decay†	Total exposure (h)
1	2·8–1·8	0·44 × 1·15 × 1·5	2·5–3·0	6:1	1·08	123
2	∞–2·8	0·40 × 0·75 × 1·2	1·5–1·6	7:1	1·08	134

* $I_{max}(0k0)/I_{min}(0k0)$ at $\chi = 90°$ for $k = 2, 6, 12, 18, 24$.
† I_o/I_f of three monitored reflections at $2\theta \sim 32°$, where I_o and I_f are the initial and final intensities respectively.

to the same shape in the range $0 \leq \rho_o \leq \chi$ and smoothly joined with a tangent from the point $\rho_o = 1$, $\rho_c = 1$. The procedure is illustrated in Fig. 3 for $\chi = 0{\cdot}35$. The value of χ used in the 2·8 Å resolution phase refinement was 0·50 but it was subsequently reduced to 0·35 in the 1·8 Å resolution phase extension and refinement. The value of $\chi = 0{\cdot}50$ suppresses regions of density below about 0·60 e Å^{-3} (~3 × r.m.s. ρ) while giving a maximum enhancement of only 12% near 1·0 e Å^{-3} and the very highest regions of electron density remain essentially unaltered. In the 1·8 Å resolution phase extension, the largest point in the electron density was about 3·7 e Å^{-3} so that a χ value of 0·35 was also suppressing density below about 0·65 e Å^{-3} (or 3 × r.m.s. ρ). This is a particularly mild modification scheme, which leads to a well behaved scale constant in refinement and effects very significant improvements in phase angles and electron density.

Two cycles of phase refinement of the 2·8 Å resolution data led to the phasing of 9745 of 9871 (98·7%) reflections with $C > 0{\cdot}15$. A region of the electron density in the active site based on these phases was examined and found to be very similar to the MIR map except for a slight general increase in density.

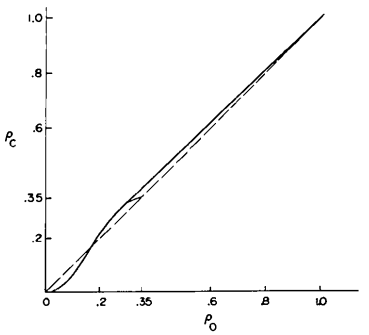

Fig. 3. Modification function for $\rho_o > 0$ and $\chi = 0{\cdot}35$. The broken line is no modification or $\rho_c(\mathbf{r}) = \rho_o(\mathbf{r})$.

Pertinent quantities and relationships used to follow the progress of this and further refinements are summarized in Table 2, from which it can be seen that the second cycle led to considerable improvement in agreement and that the average change in phase angle with respect to MIR phases after the two cycles of refinement (13·9°) is still well within the average error of the MIR phases ($\langle m \rangle = 0{\cdot}76$).

5. 1·8 Å Resolution phase extension and refinement

The modified map of cycle 2, based on 9745 refined 2·8 Å resolution phase angles, was used to initiate the phase extension to 1·8 Å resolution. The value of χ was maintained at 0·50 for this cycle; however, the value for the phase-acceptance ratio C was conservatively increased to 0·30. This led to about 1400 new phase angles beyond 2·8 Å resolution. An approximate 1·8 Å resolution map was then computed using 11 129 reflections (~56% of the data). Since the resolution of the electron density maps would be increasing hereinafter, the summation intervals were reduced at this stage from $a/54$, $b/72$, $c/72$ of the 2·8 Å resolution refinement to $a/76$, $b/100$, $c/100$ to better satisfy sampling criteria (Collins, 1975).

The progress of the refinement is summarized graphically in Fig. 4. After eight cycles of extension refinement, the phases of 19 066 (96%) reflections were determined and refined at 1·8 Å resolution. In addition to monitoring progress through the quantities shown in Fig. 4 and Table 2, small regions of the electron density map were also sampled after cycles 5 and 6. These proved to be similar to the MIR map but with increased peak heights and more detail. The same applies to the final map (cycle 10) with respect to cycles 5 and 6.

The rate of convergence of the phase extension refinement can be seen from the monotonic approach of R, $\langle \Delta\alpha \rangle$, $\langle \Delta\alpha_\omega \rangle$ and k to definite and reasonable values

Table 2. *Quantities monitored during progress of extension refinement*

Cycle number	0	1	2	3	4	5	6	7	8	9	10
R*	–	0·206	0·131	0·399	0·364	0·332	0·276	0·218	0·182	0·158	0·147
$\langle \Delta\alpha \rangle$/cycle	–	12·3	7·7	4·6	5·9	7·5	6·5	6·9	5·8	4·7	3·8
$\langle \Delta\alpha_\omega \rangle$/cycle†	–	9·3	5·5	3·4	4·4	5·2	5·0	5·3	4·4	3·6	3·0
k‡	–	1·13	1·10	1·20	1·10	1·04	1·01	1·00	1·00	1·00	1·01
χ	–	0·50	0·50	0·50	0·35	0·35	0·35	0·35	0·35	0·35	0·35
$\rho_{max}\ \chi/2$ (e Å^{-3})	–	0·62	0·64	0·68	0·48	0·52	0·59	0·65	0·65	0·65	0·65
$C = \lvert F_c \rvert / \lvert F_o \rvert$	–	0·15	0·15	0·30	0·25	0·20	0·15	0·15	0·15	0·15	0·15
Phases assigned	8 400	9 677	9 745	11 129	13 720	15 800	17 720	18 589	18 896	19 001	19 066
Fraction assigned	0·425	0·490	0·493	0·563	0·694	0·800	0·897	0·941	0·956	0·962	0·965
$\langle \lvert \alpha_{MIR} - \alpha_c \rvert \rangle$§	–	9·8	13·9	16·6	19·6	21·6	23·3	24·8	26·0	27·0	28·0

* $R = \Sigma \big| \lvert F_o \rvert - \lvert F_c \rvert \big| / \Sigma \lvert F_o \rvert$; computed for all data.
† $\langle \Delta\alpha_\omega \rangle = \Sigma \lvert F_o \rvert \Delta\alpha / \Sigma \lvert F_o \rvert$.
‡ $k = \Sigma \lvert F_o \rvert \lvert F_c' \rvert / \Sigma \lvert F_c' \rvert^2$; computed for all data.
§ Tabulated values are the modulus weighted average and are based on the 8 400 reflections in the starting set.

(Fig. 4) while constant refinement conditions were maintained. As Collins, Brice, la Cour & Legg (1976) correctly point out, the significance of such quantities lies primarily in the way they change rather than in their absolute magnitude because other factors such as the choice of χ affect the latter. Thus, 'improvements' in R, $\langle \Delta\alpha \rangle$ and $\langle \Delta\alpha_\omega \rangle$ could be attained (shift toward smaller values) quite irrespective of any improvement in the corresponding phase set. In addition, it can also be seen from Fig. 4 that extension of phase angles is essentially complete at cycle 8, when over 95% of the observed reflections were phased. Determination of more phase angles would require reducing the acceptance criterion below 0·15. Finally, from Fig. 4 it can be seen that both the ratio of $\sum |F_o| / \sum |F_c|$ and the scale constant, k, approach unity with convergence.

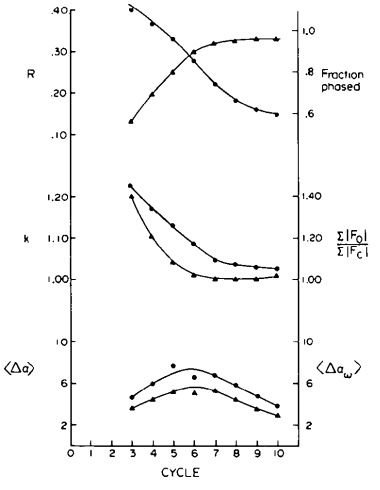

Fig. 4. Summary of phase extension refinement from 2·8 to 1·8 Å resolution. ● – $R = \sum||F_o| - |F_c||/\sum|F_o|$; ▲ – $k = \sum |F_o||F_c'|/\sum|F_c'|^2$, all reflections included; ▲ – $\langle \Delta\alpha_\omega \rangle = \sum |F_o| \Delta\alpha / \sum |F_o|$, only phased reflections included.

The behavior of the foregoing quantities was also monitored as a function of scattering angle; a representative selection of this is shown in Fig. 5. The functions of Fig. 5 were computed including only reflections that had been assigned a phase. The value of R in cycle 5 is about 0·10 for the 2·8 Å resolution data and about 0·38 for the extended phase set; the value of the latter for the previous cycle was about 0·75. As can be seen from Fig. 5, as the refinement and extension progresses, the R value of the extended set improves steadily while that of the 2·8 Å resolution set remains essentially the same. Similar trends are also observed for k and $\langle \Delta\alpha_\omega \rangle$.

The changes in R and $\langle |\alpha_{MIR} - \alpha_c| \rangle$ were also monitored as a function of $\sin\theta/\lambda$ and cycle of refinement for the 2·8 Å resolution data. The 2·8 Å resolution R remains essentially constant after onset of extension to 1·8 Å resolution and this can be seen clearly from Figs. 5 and 6. The anomalously low point of cycle 4 (R = 0·066, Fig. 6) is the result of a change in the value of χ of the modification function (Table 2) during this cycle. The average change in phase angle with respect to MIR phases is also shown in Fig. 6, from which it can be seen to be converging at about 28°. This value is well within the average error of the MIR phases ($\langle m \rangle$ = 0·76, ~40°). The general behavior of $\langle |\alpha_{MIR} - \alpha_j| \rangle$ was to increase by about 10° from the low to the high orders and to increase by about 2–3° per cycle (j) of extension refinement. The value of R decreases from about 0·09 in the low orders through a shallow minimum of about 0·07 and then increases to about 0·11 near the 2·8 Å resolution limit. Such behavior is related to the radial $|F|^2$ distribution which possesses a maximum in the vicinity of the minimum R value.

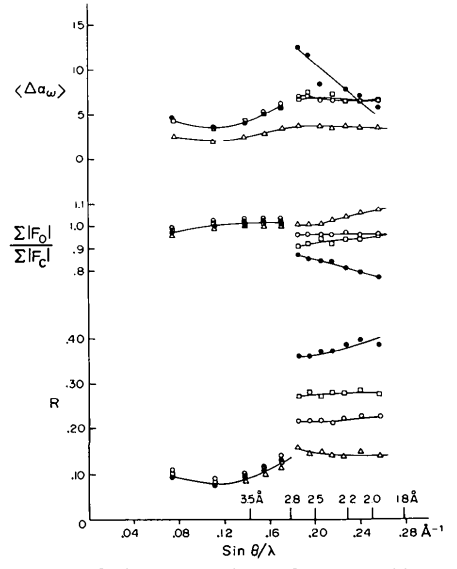

Fig. 5. Summary of phase extension refinement with respect to resolution. Quantities are as in Fig. 4; ● cycle 5, □ cycle 6, ○ cycle 7, △ cycle 10; only phased reflections included. [The magnitudes of the phase-extended reflections of the early cycles are generally small. This is related to the fact that they are identically zero for a Fourier inversion of the 2·8 Å resolution map. Since the latter is modified, this gives rise to non-zero but small structure factors beyond the 2·8 Å resolution limit.]

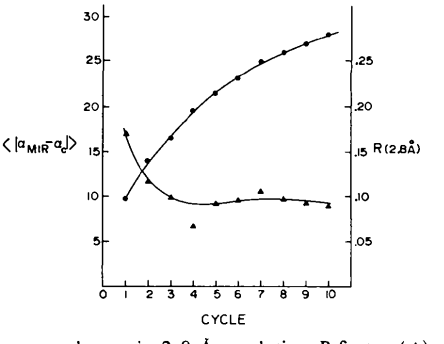

Fig. 6. Average change in 2·8 Å resolution R factor (▲) and MIR phase angles (●) with extension refinement.

A bivariate analysis of m and $|\alpha_{MIR} - \alpha_c|$ of the final cycle showed that the phase change was small when m was large. The analysis also showed that only 11 of 320 centrosymmetric 2·8 Å resolution ($h0l$) MIR-determined signs changed sign during the extension refinement. Another bivariate analysis of $|F_o|$ and $|\alpha_{MIR} - \alpha_c|$ showed that the phase change was generally small for large values of $|F_o|$.

A histogram showing the number of reflections with a given phase change from MIR phases is shown in Fig. 7 from which it can be seen that 67% of the MIR phases changed by less than the average expected error of 40°. Also shown in Fig. 7 is a histogram of the reflections satisfying the phase-acceptance criterion C, from which it can be seen that the $|F_c|/|F_o|$ distribution is fairly normal and that about 92% of the reflections calculate within 50% of their observed values. Since $|F_c|$ is obtained by Fourier inversion of a $(2|F_o| - |F_c|)$ map, $|F_c|/|F_o|$ approaches unity only as convergence is approached.

6. Refinement of the position of the local twofold axis

The transformation between the two molecules in the asymmetric unit was refined at 2·8 Å resolution by the method of least squares, minimizing the sum of the squares of the difference electron density between the independent molecules (Cohen, Matthews & Davies, 1970). The molecular boundary was approximated by defining variable rectangular yz regions as a function of the **a*** direction. The different transformations were specified by Eulerian angles, φ, ψ, θ, and translational parameters d_1, d_2, d_3 relative to a^*, b and c.†

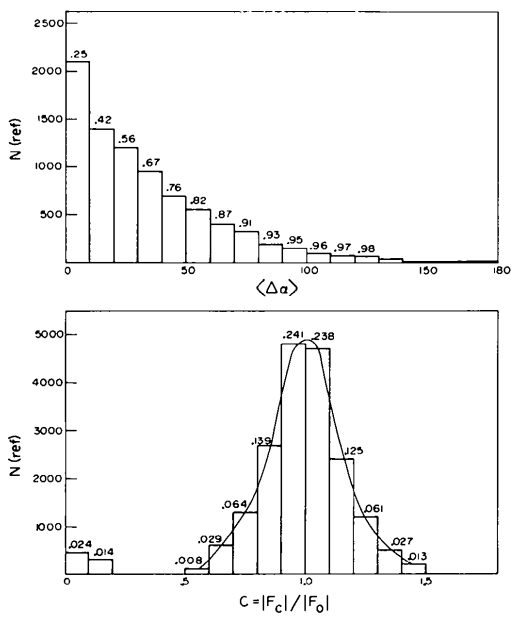

Fig. 7. Number of reflections with a given phase change from MIR phase angles (top) and distribution of $|F_c|/|F_o|$ (bottom). The expected error in MIR phases is 40° ($\langle m \rangle = 0{\cdot}76$).

A unit scale was originally assumed between the electron density of the two molecules.‡ The electron density used in the refinement was computed at intervals of 67, 100, 82 along **a**, **b**, **c** respectively (0·73, 0·67, 0·80 Å, or 274 700 points of the asymmetric unit). The transformation parameters and other quantities relating to the progress of the refinement were calculated section by section along the **a*** direction. The first cycle of refinement gave an average correlation coefficient, $\langle c_{12} \rangle$, of 0·77 for all sections, where

$$\langle c_{12} \rangle = \sum (\rho_1 - \bar{\rho}_1)(\rho_2 - \bar{\rho}_2) / [\sum (\rho_1 - \bar{\rho}_1)^2 \times \sum (\rho_2 - \bar{\rho}_2)^2]^{1/2},$$

ρ_1 and ρ_2 are the electron densities of the respective molecules and $\bar{\rho}_1$ and $\bar{\rho}_2$ their average density. The correlation coefficient converged at 0·82 in three cycles of refinement.

At this stage, it was clear from an examination of the difference electron density between the two molecules that significant differences existed between the two molecules. Since an asymmetric distribution of such differences could conceivably affect the transformation between the molecules, these regions were removed from the electron density and an additional cycle of refinement was performed. The standard deviation of the native 2·8 Å resolution electron density map is 0·18 e Å^{-3} (Dickerson, Kendrew & Strandberg, 1961; Tulinsky, Vandlen, Morimoto, Mani & Wright, 1973) and it is 0·25 e Å^{-3} for the difference density between the two molecules ($\Delta\rho_{12}$). Therefore, all regions with $|\Delta\rho_{12}| > 0{\cdot}7$ e Å^{-3} (approximately 40 000 points or 16% of the density) were removed from the density for the next cycle of refinement. This produced a significant improvement in correlation to 0·86; however, the transformation parameters remained essentially the same as those of the previous cycle indicating that the distribution of lack of twofold symmetry was not generally asymmetric with respect to the position of the local twofold axis. A comparison of the transformation parameters with the previous position of the local twofold axis gave no indication that the symmetry operation relating the two molecules departed significantly from being a twofold axis parallel to **a***.

The electron density distributions of tosylated α- and γ-CHT have been compared at 5·5 Å resolution by Cohen, Matthews & Davies (1970). The correlation coefficient between the independent molecules of α-

† A consequence of this choice of axes is that a rotation of 180° about **a*** leads to a singularity in the rotation matrix. This will give rise to abnormally large standard deviations in φ and θ.

‡ Since the average density of the individual molecules was calculated to be the same after the first cycle of refinement, this parameter was maintained at unity throughout the remainder of the refinement.

CHT was only 0·77, suggesting a much smaller value at 2·8 Å resolution than that obtained here for the native enzyme. Moreover, the correlation between the α- and γ-CHT structures was of comparable quality. Since we observe about 16% of the density between the two molecules to be significantly different, the α–γ CHT comparison at lower resolution does not preclude significant differences between the α- and γ-CHT structures at higher resolution.

On extension of the refinement to 1·8 Å resolution, the correlation coefficient decreased to 0·606. In order to minimize interpolation errors, the summation grid of the 1·8 Å resolution map was reduced to 76 × 106 × 130 (0·65 × 0·61 × 0·51 Å) or 523 640 points per asymmetric unit. A cycle of refinement did not alter the correlation appreciably (0·614) and since the position of the local twofold axis remained the same within the error of its determination, the refinement was considered converged. The equation defining the position of the local twofold axis is $z = (0{\cdot}152 \pm 0{\cdot}003)x + (0{\cdot}380 \pm 0{\cdot}003)$, with $y = 0{\cdot}309 \pm 0{\cdot}002$. This equation does not differ very significantly from that of Birktoft & Blow (1972) or that previously determined at 2·8 Å resolution (part I).

Quantities which were used to monitor the progress of the refinement are listed in Table 3. These were also computed in sections perpendicular to **a*** and generally plotted and examined with respect to this direction. From the behavior of the correlation coefficient along the twofold axis, the quality of the twofold symmetry is essentially constant throughout the molecule but deteriorates significantly 7–8 Å from the surface.

The refinement of the transformation parameters was carried out using all the points within the defined molecular volume and also using a smaller number of points which satisfied a minimum value of the electron density (*e.g.* above the expected error). The two modes of refinement gave the same results for the position of the twofold axis. The values of 37·3 and 38·7% of the total number of points in Table 3 should be compared to about 60% which represents the amount of protein by weight in crystals. Thus, the molecular volume was chosen conservatively for the calculations. The decrease in the fraction of points greater than the expected error from 23·3 to 15·5% with increased resolution is due to an overall sharpening of the electron density.

Table 3. *Summary of local twofold refinement*

d_{min} (Å)	2·8	2·8	1·8	1·8
ρ_{min} (e Å^{-3})*	/	0·25	/	0·40
Σ†	102 468	63 780	202 813	81 371
Fraction (%)‡	37·3	23·2	38·7	15·5
$\langle c_{12} \rangle$	0·78	0·82	0·58	0·61
$\langle \rho_1 \rangle$ (e Å^{-3})	0·26	0·42	0·26	0·62
$\langle \rho_2 \rangle$ (e Å^{-3})	0·26	0·41	0·26	0·60
r.m.s. $\Delta\rho$ (e Å^{-3})4¶	0·27	0·30	0·49	0·72

* Minimum value of electron density considered; all points within the molecular volume or ρ_{min}.

† Number of points with $\rho > \rho_{min}$.

‡ Fraction of points in asymmetric unit.

¶ r.m.s. $\Delta\rho = \sum(|\rho_1 - \rho_2|^2/N)^{1/2}$, where N is the number of points.

The average over all points within the molecular boundary is $F(000)/V = 0{\cdot}252$ e Å^{-3}, where $F(000)$ is the number of electrons in α-CHT and V is the volume of the molecule. From the average density for points with $\rho > 0{\cdot}4$ e Å^{-3}, it can be seen from Table 3 that the scale between the two molecules is close to unity. The r.m.s. $\Delta\rho$, which reflects the discrepancies between the two molecules, is only slightly greater than the expected error at 2·8 Å resolution but is significantly greater at higher resolution [$\sigma(\rho) \sim 0{\cdot}25$ e Å^{-3} at 1·8 Å resolution or $\sigma(\Delta\rho) \sim 0{\cdot}35$ e Å^{-3}]. This is consistent with the decrease in correlation as the resolution is increased.

The largest electron densities in the 1·8 Å resolution map ranged from 3·2 to 3·8 e Å^{-3} and these were generally associated with disulfides of Cys residues. The more prominent features of the map, such as the polypeptide chains, hovered around 2·5 e Å^{-3}. The largest differences between the two molecules were 2·0 e Å^{-3} and significant differences averaged near ±1·0 e Å^{-3}.

A bounded section (3·2 Å) of the 1·8 Å resolution map perpendicular to and including the local twofold axis is shown in Fig. 8. This region, showing distinct lack of twofold symmetry, is a typical example of such regions and has been discussed previously at the 2·8 Å resolution level (Tulinsky, Vandlen, Morimoto, Mani & Wright, 1973). It occurs in the dimer interface region and contains the main chain from Trp 215 to Ser 218. From Fig. 8, it can be seen that the lack of symmetry persists at 1·8 Å resolution and a comparison with the 2·8 Å resolution map shows that it is even more

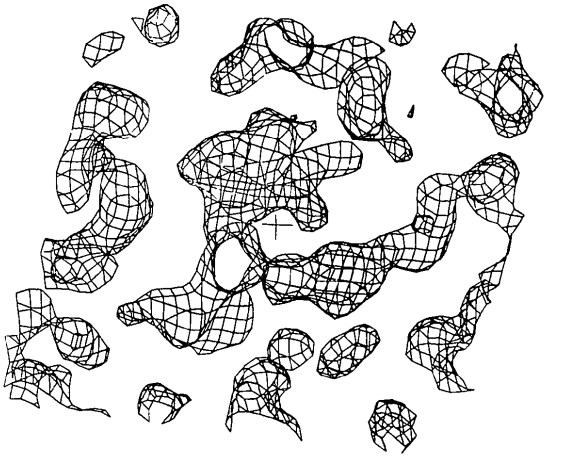

Fig. 8. Bounded section (3·2 Å) of 1·8 Å resolution map viewed down **a***. Basket contour at 0·6 e Å^{-3}; local twofold axis designated by cross; apparent holes and incomplete basket contour due to abrupt cut-off of density at sections $\chi = 37$ and 41/76.

pronounced than previously noted. The region was originally interpreted as corresponding to two chains approximately parallel to each other with one chain approaching the local twofold axis within 1·75 Å (above the twofold axis) while the other remains more distant at 4·0 Å (below the twofold axis). In addition, the chains are displaced by about 2·0 Å with respect to each other along the twofold direction and this can even be seen from the basket contour map of Fig. 8.

Although Rossmann (1976) has suggested that the 2·8 Å resolution results showing lack of twofold symmetry might be due to 'the large number of closely linked parameters', no further explanation was presented concerning the nature of these parameters or how they might be a source of asymmetry. Presumably, the parameters are some of those used by us in the MIR method. However, since the tosyl-α-CHT structure determination was based on a similar set of MIR parameters (Blow & Matthews, 1973), yet the structure showed considerably less asymmetry, it would seem that the lack of symmetry in the present case is independent of the heavy-atom parameters and further proof is required before they can be implicated in the asymmetry. The extension of phase angles to 1·8 Å resolution has been carried out using a different method of phase determination which depends only indirectly on such parameters. Since the lack of twofold symmetry not only persists but generally increases with the increased resolution, a behavior to be expected if the effect were in fact real, it appears that the original lack of symmetry is not a heavy-atom artifact of the MIR phase determination. Finally, and most importantly, it should be noted that the details of the asymmetry are biochemically reasonable and also very informative (Tulinsky, Vandlen, Morimoto, Mani & Wright, 1973) and that the asymmetric response of the dimeric molecule in certain interactions with small molecules is now a well documented behavior (Mavridis, Tulinsky & Liebman, 1974; Tulinsky, Mavridis & Mann, 1978).

7. Comparison of the 2·8 Å and 1·8 Å resolution maps

A representative bounded section (3·9 Å) of the 2·8 Å resolution MIR map is shown in Fig. 9 along with its 1·8 Å resolution phase-extended counterpart. These maps correspond to a region on the surface of the protein essentially composed of extended chains involved in distorted β-sheet formation (Val 66–Gly 74, Thr 110–Thr 117 and Lys 84–Ile 85). From Fig. 9, it can be seen that the peak heights of the 1·8 Å resolution map are generally one and a half times greater than those of the 2·8 Å resolution map, that the general aspects of the two maps are similar and that there is an obvious enhancement in resolution (*e.g.* regions 66–72, 113–117) in the 1·8 Å resolution map. Such behavior is representative and pervades the 1·8 Å resolution map.

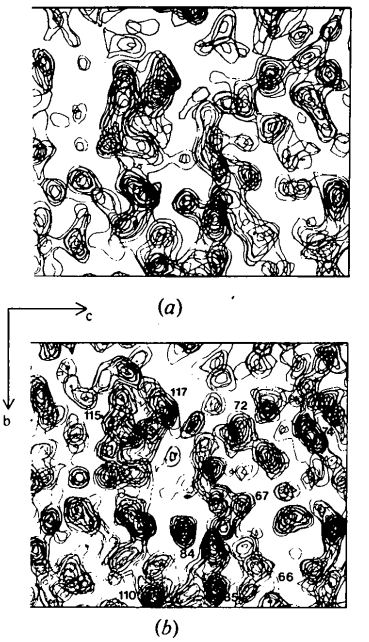

Fig. 9. Comparison of bounded sections (3·9 Å) viewed down **a*** (0–6/76) of (*a*) 2·8 Å resolution MIR map and (*b*) 1·8 Å resolution phase-extended map. Contours at 0·4 e Å^{-3} beginning with 0·4 e Å^{-3}; some regions of main chain numbered in (*b*).

The 2·8 Å resolution map proved to be in agreement with previous observations at this resolution which showed that polypeptide chains are observed as columns of continuous high density with prominent peaks marking the branching points of side chains, whereas at 1·8 Å resolution prominent peaks develop along the backbone which correspond to peptide carbonyl groups (North & Phillips, 1969; Podjarny, Yonath & Traub, 1976). This has aided us in orienting the peptide units. At 1·8 Å resolution, there are also occasional narrow ribbons of weak density (1·0–1·2 e Å^{-3}) between carbonyl and imino groups obviously involved in hydrogen-bonding situations. Aromatic residues were generally recognized with ease in the 2·8 Å resolution map from the high density usually associated with them; in the 1·8 Å resolution map, this density tended to be flatter compared to the 2·8 Å map. A good example of such behavior occurs in the tripeptide sequence Trp 27–Pro 28–Trp 29, where the density of the indoles (2·0–2·5 e Å^{-3}) is particularly unambiguous. Cysteine disulfide bridges (~2·2 e Å^{-3}) were difficult to distinguish from the main chain direction at 2·8 Å resolution whereas the S atoms of the disulfide bridges between Cys 1–122 (3·2 e Å^{-3}), Cys 42–58 (2·8 e Å^{-3}) and Cys 190–221 (3·2 e Å^{-3}) are practically resolved in the 1·8 Å resolution map. The generally larger density of S atoms also helps identify localized sulfate ions in the 1·8 Å map which were originally inferred from isomorphous sulfate–selenate exchange experiments (Tulinsky & Wright, 1973).

In the 2·8 Å resolution map, the density of the side chains of the *A* chain of α-CHT was weak (1·0–1·5 e Å^{-3}) and ambiguous and there was no definite density observed for Leu 10–Leu 13 (Vandlen, 1972). In the 1·8 Å map, the side-chain density for Leu 10–Gly 12 is present (1·0–2·3 e Å^{-3}) and clearly defined; however, there is still no density corresponding to Leu 13. In addition, there is well defined density for Ile 6–Gln 7 which was diffuse in the 2·8 Å resolution map.

Side chains such as Lys, Arg, Gln, that are on the surface of the molecule, often had weak density indicating them in the 2·8 Å map. The density for these side chains in the 1·8 Å map appears to be generally improved. In fact, some of these side chains are not in a single position but adopt different orientations and/or conformations in different molecules in the crystal making the corresponding electron density appear to be weak.

Finally and importantly, the conformations of the residues of the catalytic triad of His 57, Asp 102 and Ser 195 in the 1·8 Å resolution map are the same as those inferred originally from the 2·8 Å map. The side-chain density of Ser 195 is large and clear in the 1·8 Å map (2·0 e Å^{-3}) and the orientation of the side chain has Oγ in the 'down' position (Birktoft & Blow, 1972; Matthews, Alden, Birktoft, Freer & Kraut, 1977). This orientation is different from that inferred by Birktoft & Blow (1972) but, as already mentioned by Matthews *et al.* (1977), it is similar to that found in other serine proteases.

We are currently refitting a Kendrew model of the dimeric molecule to the 1·8 Å resolution map and remeasuring the model coordinates. The coordinates of this model will be idealized and refined further before final detailed comparisons are made of the similarities and asymmetry between the two independent molecules of the asymmetric unit of α-CHT.

8. Summary comments: density-modification refinement extension

Without a doubt, the single most important consideration in the present density modification scheme was the proper choice of the χ parameter which is related to the maximum value of the electron density which is suppressed by the procedure. The use of the χ parameter is required whenever the electron density function is not of fairly uniform height, as when heavier elements are present (Collins, Brice, la Cour & Legg, 1976) or even in the presence of S atoms of Cys and Met residues. If such a procedure is not used or if it is underestimated, repeated application of a modification function such as (1) will result in a spurious growth of the higher density at the expense of the remainder. We originally employed a value of $\chi = 0{\cdot}7$, which suppressed density $<0{\cdot}87$ e Å^{-3} [$\sim 4{\cdot}8\sigma(\rho)$] in the 2·8 Å resolution map (Raghavan & Tulinsky, 1977). After iterative phase extension, we discovered that the density of the main chain of α-CHT practically doubled whereas the side chains, which were initially of generally lower density, either remained essentially the same or in some cases even decreased. The most perturbing aspect of this behavior was the fact that the parameters and criteria used to monitor the progress of the refinement did not indicate any apparent difficulties. A suitable compromise for the choice of χ was attained with a value of 0·35 which suppressed density $<0{\cdot}6$ e Å^{-3} and which was close to the $3\sigma(\rho)$ limit.

A most important consideration in monitoring the progress of a refinement extension is that of maintaining constant density-modification refinement-extension parameters or altering them only with discretion. The significance of such parameters generally lies in the manner in which they change rather than in their absolute values because other factors might be influencing them (*e.g.* choice of χ). Thus, favorable shifts in quantities such as R, $\langle \Delta\alpha \rangle$ and $\langle \Delta\alpha_\omega \rangle$ might be realized irrespective of improvements in a phase set. This can be seen clearly for cycle 4, from Fig. 6 and Table 2, and results from a change in χ during this cycle.

In retrospect, we could probably have improved the density-modification function by replacing the solvent density beyond the first or second solvation sphere of the protein with that of its average value in a manner similar to that used in non-crystallographic symmetry refinement-extension applications (Argos, Ford & Rossmann, 1975; Bricogne, 1976). This would have had the effect of attenuating the solvent density as its distance from the protein surface increased. Without such a modification, it appears that some of the far-removed solvent is more enhanced than expected. However, these regions are usually of minimal consequence in interpretation and in affecting the phase angles (only the lowest-order reflections are involved).

Although it is clear that it is possible to extend phase angles beyond a given resolution based on a limited set of phases (Kartha, 1969; Sayre, 1974; Collins, Brice, la Cour & Legg, 1976), it is equally clear that the initial set of known phases must be sufficiently large. Less clear is the relationship between the size of the starting set and the phase extension possible thereof. In the present case, a starting set of phase angles between 2·5 and 2·2 Å resolution would probably have led to more improved resolution in the final 1·8 Å resolution map. The effect of starting with the smaller 2·8 Å resolution set of phases appears to be that of a mild smearing of the higher-resolution map. Starting with an even smaller set (~3·0 Å resolution) would probably have led only to an enhancement of the unresolved map without any improvement in resolution. Finally, although the results of the extension of phase angles by density modification and other methods are critically dependent

upon the size of the starting set of phases, this is not so for the refinement of a given set of phase angles by electron density modification. In this case, significant improvement in phase angles can be accomplished at any resolution by performing a small number of cycles of inverse transform calculations of a suitably modified density. This could prove to be an expeditious way to additionally improve MIR 'best' electron density maps.

We would like to thank Dr David J. Duchamp, The Upjohn Company, Kalamazoo, Michigan, for Cal-Comp drawings of the 1·8 Å resolution map at Kendrew-model scale. We would also like to thank Dr S. R. Ernst for his help and discussions of various computational problems throughout this work. This work was supported by NIH grants GM21225-01,02,03.

References

ARGOS, P., FORD, G. C. & ROSSMANN, M. G. (1975). *Acta Cryst.* A**31**, 499–506.

AUNE, K. C. & TIMASHEFF, S. N. (1971). *Biochemistry*, **10**, 1609–1617.

BARRETT, A. N. & ZWICK, M. (1971). *Acta Cryst.* A**27**, 6–11.

BIRKTOFT, J. J. & BLOW, D. M. (1972). *J. Mol. Biol.* **68**, 187–240.

BLOW, D. M. & CRICK, F. H. C. (1959). *Acta Cryst.* **12**, 794–802.

BLOW, D. M. & MATTHEWS, B. W. (1973). *Acta Cryst.* A**29**, 56–62.

BLOW, D. M., ROSSMANN, M. G. & JEFFERY, B. A. (1964). *J. Mol. Biol.* **8**, 65–78.

BRICOGNE, G. (1976). *Acta Cryst.* A**32**, 832–847.

COHEN, G. H., MATTHEWS, B. W. & DAVIES, D. R. (1970). *Acta Cryst.* B**26**, 1062–1069.

COLLINS, D. M. (1975). *Acta Cryst.* A**31**, 388–389.

COLLINS, D. M., BRICE, M. D., LA COUR, T. F. M. & LEGG, M. J. (1976). *Crystallograhic Computing Techniques*, edited by F. R. AHMED, pp. 330–335. Copenhagen: Munksgaard.

COLLINS, D. M., COTTON, F. A., HAZEN, E. E. JR, MEYER, E. F. JR & MORIMOTO, C. N. (1975). *Science*, **190**, 1047–1053.

DICKERSON, R. E., KENDREW, J. C. & STRANDBERG, B. E. (1961). *Acta Cryst.* **14**, 1188–1195.

HOPPE, W., GASSMANN, J. & ZECHMEISTER, K. (1970). *Crystallographic Computing Techniques*, edited by F. R. AHMED, pp. 96–102. Copenhagen: Munksgaard.

KARTHA, G. (1969). *Acta Cryst.* A**25**, S87.

MATTHEWS, D. A., ALDEN, R. A., BIRKTOFT, J. J., FREER, S. T. & KRAUT, J. (1977). *J. Biol. Chem.* **252**, 8875–8883.

MAVRIDIS, A., TULINSKY, A. & LIEBMAN, M. N. (1974). *Biochemistry*, **13**, 3661–3666.

NORTH, A. C. T. & PHILLIPS, D. C. (1969). *Prog. Biophys.* **19**(1), 5–132.

PODJARNY, A. D., YONATH, A. & TRAUB, W. (1976). *Acta Cryst.* A**32**, 281–292.

RAGHAVAN, N. V. & TULINSKY, A. (1977). Am. Crystallogr. Assoc. Summer Meeting, East Lansing, Michigan, Abstract PB 22.

ROSSMANN, M. G. (1976). *Acta Cryst.* A**32**, 774–777.

SAYRE, D. (1974). *Acta Cryst.* A**30**, 180–184.

TEN EYCK, L. F. (1973). *Acta Cryst.* A**29**, 183–191.

TULINSKY, A., MANI, N. V., MORIMOTO, C. N. & VANDLEN, R. L. (1973). *Acta Cryst.* B**29**, 1309–1322.

TULINSKY, A., MAVRIDIS, I. & MANN, R. F. (1978). *J. Biol. Chem.* **253**, 1074–1078.

TULINSKY, A., VANDLEN, R. L., MORIMOTO, C. N., MANI, N. V. & WRIGHT, L. H. (1973). *Biochemistry*, **12**, 4185–4193.

TULINSKY, A. & WRIGHT, L. H. (1973). *J. Mol. Biol.* **81**, 47–56.

VANDLEN, R. L. (1972). PhD Thesis, Michigan State Univ.

VANDLEN, R. L. & TULINSKY, A. (1973). *Biochemistry*, **12**, 4193–4200.

WYCKOFF, H. W., DOSCHER, M., TSERNOGLOU, D., INAGAMI, T., JOHNSON, L. N., HARDMAN, K. D., ALLEWELL, N. M., KELLY, D. M. & RICHARDS, F. M. (1967). *J. Mol. Biol.* **27**, 563–578.

Acta Cryst. (1979). B**35**, 1785–1790

Crystal Structures of Two Forms of 1,2-Bis(diphenylphosphino)ethane

BY CORRADO PELIZZI AND GIANCARLO PELIZZI

Istituto di Chimica Generale ed Inorganica, Centro di Studio per la Strutturistica Diffrattometrica del CNR, Parma, Italy

(*Received* 12 *October* 1978; *accepted* 14 *March* 1979)

Abstract

Crystals of both forms of the title compound, $C_{26}H_{24}P_2$, are monoclinic (space group $P2_1/n$) with unit-cell dimensions a = 13·154 (7), b = 5·508 (4), c = 15·960 (8) Å, β = 110·75 (6)°, Z = 2 for form (I) and a = 9·078 (9), b = 5·763 (4), c = 21·314 (12) Å, β = 100·78 (4)°, Z = 2 for form (II). The structures were both solved from X-ray diffractometer data with direct methods for (I) and the heavy-atom technique for (II). Refinement by full-matrix least squares gave R = 4·37% for 1257 independent reflections and R =

0567-7408/79/081785-06$01.00